Random Forest Based Left Ventricle Segmentation in LGE-MRI

Tanja Kurzendorfer[1], Christoph Forman[2], Alexander Brost[3] and Andreas Maier[1]

[1] Pattern Recognition Lab, Friedrich-Alexander University Erlangen-Nuremberg, Erlangen, Germany
tanja.kurzendorfer@fau.de
[2] Siemens Healthcare GmbH, Erlangen, Germany
[3] Siemens Healthcare GmbH, Forchheim, Germany

Abstract. The leading cause of death worldwide is ischaemic heart disease. Late gadolinium enhanced magnetic resonance imaging (LGE-MRI) is the clinical gold standard to visualize regions of myocardial scarring. However, the challenge arises in the segmentation of the myocardial border, as the transition of scar tissue and blood pool can be very smooth, because the contrast agent accumulates in the damaged tissue and leads to various enhancements. In this work, a random forest based boundary detection approach is combined with a scar exclusion criterion. The final endocardial and epicardial border is found with the help of dynamic programming, which finds the distance weighted minimum through the boundary cost array. The segmentation method is evaluated using a 5-fold cross validation on 100 clinical LGE-MRI data sets. The Dice coefficient resulted in an overlap of 0.83 for the endocardium as well as for the epicardium.

1 Introduction

The leading cause of death worldwide is ischaemic heart disease [1]. For diagnosis in clinical routine cardiac magnetic resonance imaging is used, as it can provide information on morphology, tissue characterization, blood flow or perfusion [2,3]. The clinical gold standard for the assessment of myocardial viability is late gadolinium enhanced magnetic resonance imaging (LGE-MRI) [4]. The enhancement of the damaged tissue is based on the different contrast agent accumulation within the tissue, which is based on T_1 weighted imaging [5]. Therefore, necrotic tissue has high signal intensity, whereas the boundaries of the myocardium are hardly enhanced. Consequently, the challenge is the accurate and reliable segmentation of the myocardium for further tissue analysis. As the quantification of the myocardial scar is needed for diagnosis, therapy planning and patient prognosis.

Most segmentation approaches for LGE-MRI require the prior delineation of the myocardium in Cine-MRI data of the same patient which are then propagated to the LGE-MRI [6,7,8,9]. However, this contour propagation has several

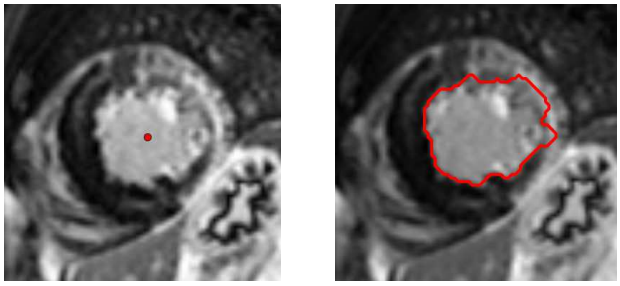

(a) Detected center (b) MACWE

Fig. 1. (a) Detected center of the left ventricle using circular Hough transforms and circularity constraints. (b) Result of the morphological active contours without edges approach (MACWE).

limitations. The cardiac phases from the Cine-MRI and the LGE-MRI may not accurately match. Inter-slice shifts from multiple breath holds can arise. The global position of the heart may change due to patient movement as contrast has to be injected and the acquisition is done 10 to 20 minutes after injection. Although these shifts may appear minor, they can lead to significant errors in the scar quantification.

Thus, we propose a random forest based segmentation approach for 2-D LGE-MRI, which is independent of Cine MRI. The major contribution of this approach is, that steerable features are extracted in polar space for the endocardial and epicardial boundary respectively. These features are used to train two random forest classifiers, which results in two boundary probability maps for the endocardium and epicardium, respectively. For the endocardium an additional scar exclusion step is added. The final segmentation result is obtained by a dynamic programming approach in polar space.

2 Materials and Methods

The segmentation of the left ventricle can be divided into several steps. First, the left ventricle is detected using a combination of circular Hough transforms, Otsu thresholding and circularity measures. In the second step, a region of interest is identified using morphological active contours. In the third step, potential endocardial boundary positions are detected by casting rays in a cylindrical fashion. The boundary probability is estimated using a random forest classifier. In addition, potential scar areas are excluded from the boundary probabilities. In the final step, the optimal contour is obtained by applying a minimal cost path search to the boundary cost array in polar space.

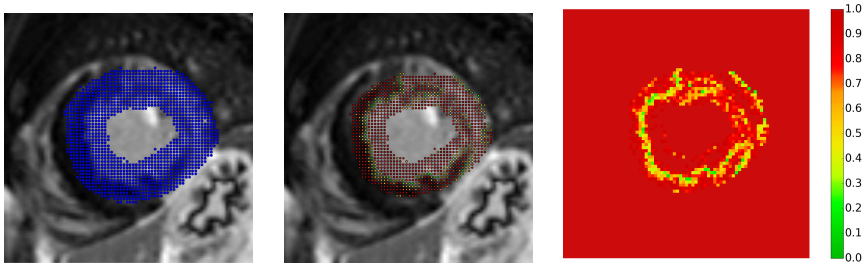

(a) Boundary candidates (b) Boundary detection (c) Boundary costs

Fig. 2. (a) Potential boundary candidates, extracted using ray casting. (b) Boundary detection result obtained from the trained random forest classifier. (c) Boundary cost map in Cartesian coordinates.

2.1 Left Ventricle Detection

The left ventricle is detected in the mid slice of the 2-D LGE-MRI stack. First, the Canny edge detector is used to extract the edges from the image [10]. In the next step, circular Hough transforms are applied [11]. The radii of the circular Hough transforms were in range of 17 mm to 35 mm with a step size of 2 mm due to performance, which was defined according to the anatomical information in literature [12]. The most prominent candidate is selected as potential left ventricle blood pool candidate. To verify this position, an additional roundness measure is applied. Therefore, Otsu's thresholding is applied to the whole slice, to convert the image into a binary mask [13]. Objects that are smaller than a predefined threshold $\theta_o = 25$ are removed. The threshold was defined heuristically. From the remaining objects the eccentricity, i.e. the roundness is estimated $R = \sqrt{\frac{a^2-b^2}{a^2}}$, where a is the semi-major axis and b is the semi-minor axis of the object. If the object is circular, $R = 0$. If the center points c_1 and c_2 of the roundest object and the result of the circular Hough transform are within θ_c, where $\theta_c = \sqrt{(c_1 - c_2)^2}$, the left ventricle has been accurately detected. Otherwise, the user is asked to verify the center of the left ventricle. The result of the left ventricle detection is shown in Fig. 1 (a).

2.2 Endocardial Boundary Estimation

After the left ventricle is detected in the center slice of the MRI stack, this information is used for the boundary detection of the endocardium. The mid-slice is a good slice to start with the segmentation, as the result can be used to propagate in basal and apical direction. To get a rough estimate of the blood pool outline, a morphological active contours without edges (MACWE) approach is applied [14]. This approach alone is not sufficient to get the outline of the blood pool as in LGE-MRI the transition between blood pool and myocardial scar

(a) Polar image

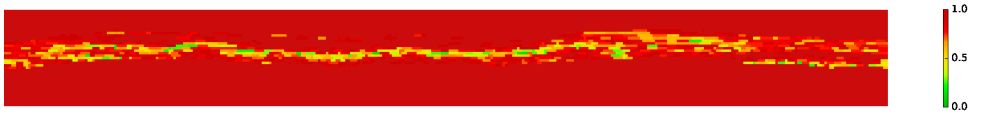

(b) Boundary costs

(c) Scar candidates

(d) Scar map

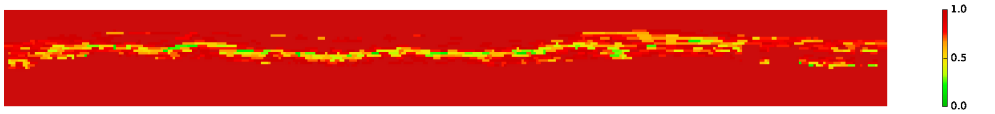

(e) Boundary cost combined with scar map

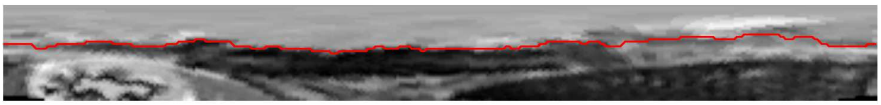

(f) MCP result

Fig. 3. (a) Mid slice image after polar transformation. (b) Boundary cost map obtained from the trained random forest classifier in polar coordinates. (c) Potential scar candidates which have an intensity value greater than θ_{st} and are not within the blood pool. (d) Scar map, where all scar candidates with increasing radius are labeled with 1. (e) Final endocardial boundary cost map, resulting from the combined boundary detection result and the scar map. (f) Final result of the minimal cost path (MCP) search in polar coordinates.

can be very smooth, see Fig. 1 (b). However, it gives us a rough outline of the

blood pool. This outline can be used to extract potential endocardial boundary candidates using circular ray casting. Therefore, the image is converted to polar coordinates. Boundary candidates are then selected for N equidistant points along R rays, as depicted in Fig. 2 (a) in Cartesian coordinates. Each potential boundary candidate is then classified using a trained random forest classifier. The result of the classification is illustrated in Fig. 2 (b) as cost map.

Boundary Map Generation: The performance of any classifier is limited by the discriminative power of the features used for training. Steerable features were used [15], as they are computationally efficient and can capture the orientation and scale. In total 16 features were extracted for each boundary candidate, based on local intensity and gradient, which result in a feature vector $\boldsymbol{x} \in \mathbb{R}^{1\times 16}$, that is used for training and detection. For a given boundary candidate $\boldsymbol{p}(x, y)$ with the intensity I and the gradient $\boldsymbol{g} = (g_x, g_y)$, the following features are extracted: I, $\sqrt{I}$, $\sqrt[3]{I}$, I^2, I^3, $\log I$, $||\boldsymbol{g}||$, $\sqrt{||\boldsymbol{g}||}$, $\sqrt[3]{||\boldsymbol{g}||}$, $||\boldsymbol{g}||^2$, $||\boldsymbol{g}||^3$, $\log ||\boldsymbol{g}||$, g_x, g_y, $\sqrt{g_x^2 + g_y^2}$, $\mathrm{div}(\boldsymbol{g})$. Note, that all the features are extracted in polar space, which is the steerable space. The center position in Cartesian space, i.e. origin in polar space, has not influence on the classification result.

The training of the random forest is based on ground truth annotations from which positive as well as negative samples are extracted. For the training pathologic as well as healthy subjects are used, to generate a broad range for the training data base. After the training, the classifier can predict the endocardial boundary probability $p_{\mathrm{endo}}(\boldsymbol{x}) \in [0, 1]$. The endocardial boundary probability can be interpreted as costs c, where $c = 1 - p_{\mathrm{endo}}$. If the boundary probability is very high, the costs are close to 0.

To improve the detection of the boundaries from scarred myocardium, an additional scar exclusion step is added. Given the mean intensity of the blood pool μ_{bp} and the standard deviation σ_{bp}, the scar threshold θ_{st} is defined as $\theta_{st} = \mu_{bp} + \sigma_{bp}$. All the pixels above this threshold and outside of the blood pool are defined as potential scar candidates, see Fig. 3 (c). The scar map is generated from the scar candidates, where all pixels with increasing radius from potential scar candidates are labeled with 1, as depicted in Fig. 3 (d). If a boundary probability overlaps with the scar map, the boundary potentials are impaired, see Fig. 3 (e).

Segmentation: In the next step, the final segmentation result of the endocardial contour has to be obtained from the endocardial cost map. Therefore, a dynamic programming approach is used in polar space, to compute the optimal endocardial contour from one end to the other end of the polar image [16]. The minimal cost path (MCP) search is used [17], which finds the distance weighted minimum path through the cost array. The cost path is calculated as the sum of the costs for each move and weighted by the length of the path. The result of the MCP is shown in Fig. 3 (f). After the optimal path is found, the contour is transfered back to Cartesian coordinates, see Fig. 4 (a). The convex hull is

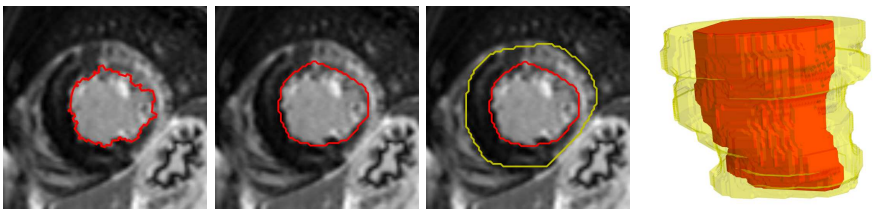

(a) Result MCP (b) Convex hull (c) Final result (d) 3-D modell

Fig. 4. (a) Result of the minimal cost path search in Cartesian coordinates. (b) Convex hull of the final result. (c) The final result of the boundary estimation for the endocardium in red and the epicardium in yellow. (d) 3-D model of the endocardial and epicardial contour in red and yellow, respectively.

calculated from the contour, as papillary muscles close to the endocardial border might be included, as visualized in Fig. 4 (b).

After the contour is refined in the mid-slice, the information is used for the boundary detection in apical and basal direction. The center is propagated to the succeeding slices and the MACWE is initialized. The boundary detection using the random forest classifier, the scar map generation, and the MCP is repeated for all succeeding slices until the base and apex is reached.

2.3 Epicardial Boundary Estimation

After the endocardial contour is found, the epicardial contour can be estimated. The segmentation starts again with the mid-slice and the result of the refined endocardial contour is used as an initialization for the boundary detection.

Again a random forest classifier is trained for the epicardial boundary detection using the same 16 features as for the endocardial border estimation, resulting in an epicardial boundary probability $p(\boldsymbol{x})_{\text{epi}}$. The result of the epicardial boundary detection is used as cost array for the minimal cost path search. The MCP is applied in polar coordinates for the same reasons as mentioned before. The MCP finds the distance weighted minimal path from the left to the right end of the polar image. The result is then transfered back to Cartesian coordinates and the convex hull is taken. The result is depicted in Fig. 4 (c).

The endocardial contour estimation is repeated till the apex and base is reached. Afterwards the contours are extracted as 3-D surface models using the marching cubes algorithm [18]. The output is a list of vertices and faces which are saved in the *.stl or *.obj file format. Fig. 4 (d) shows an example of a 3-D surface mesh, where the endocardium is visualized in red and the epicardium in yellow.

	Endo	Epi	Inter Endo	Inter Epi
Dice	0.83 ± 0.08	0.83 ± 0.08	0.95 ± 0.06	0.96 ± 0.05
MSD	3.55 ± 2.08	4.12 ± 2.11	0.89 ± 1.14	0.93 ± 1.13

Table 1. Segmentation results for the endocardium (Endo), epicardium (Epi) and inter observer variability using the Dice coefficient and the mean surface distance.

3 Evaluation and Results

The automatic segmentation of the left ventricle's endo- and epicardium was evaluated on 100 clinical LGE-MRI data sets. The inversion recovery 2-D LGE-MRI sequences were acquired with a Siemens MAGNETOM Area 1.5T scanner (Siemens Healthcare GmbH, Erlangen, Germany). The slice thickness was 8-10 mm, with a pixel size of (1.59-2.08 × 1.59-2.08) mm^2 and the spacing between the slices was set to 10 mm. Each data set contained between 10 and 13 short axis slices. Gold standard annotations of the LV endo- and epicardium were provided by two clinical experts. The annotations were preformed using MITK [19]. The observers were asked to outline the endocardial and epicardial contour separately.

Given the gold standard annotations, the segmentation was evaluated using different measures, the volumetric Dice coefficient (DC) and the mean surface distance (MSD). Furthermore, the inter-observability was evaluated. The evaluation itself was performed by a 5-fold cross validation, e.i. 20 sequences were excluded from the training of the random forest classifier and used for testing. In Table 1 the average values and the standard deviation of the computed metrics are presented for the endocardium and epicardium. In Fig. 5 the qualitative results of the segmentation are presented. The first row depicts the raw data from base to apex. The second row shows the gold standard annotation of one clinical expert, where the endocardial contour is orange and the epicardial contour green. The last row illustrates the result of the proposed segmentation algorithm, where the endocardium is red and the epicardium yellow.

The proposed approach was implemented in Python (single threaded, no optimization) and needs less than 10 seconds for the entire segmentation on a computer equipped with an Intel i7 2.8 GHz CPU and 16 GB of RAM.

4 Discussion and Conclusion

The presented work solely uses LGE-MRI data for the segmentation of the left ventricle, compared to most work reported in literature, which make use of Cine MRI and propagate the contours [6,7,8,9]. Albà et al. [20] computed directly the contours from LGE-MRI. Our results are in the same range of the reported errors in literature. However, a direct comparison to the method is not possible, as the data sets differ.

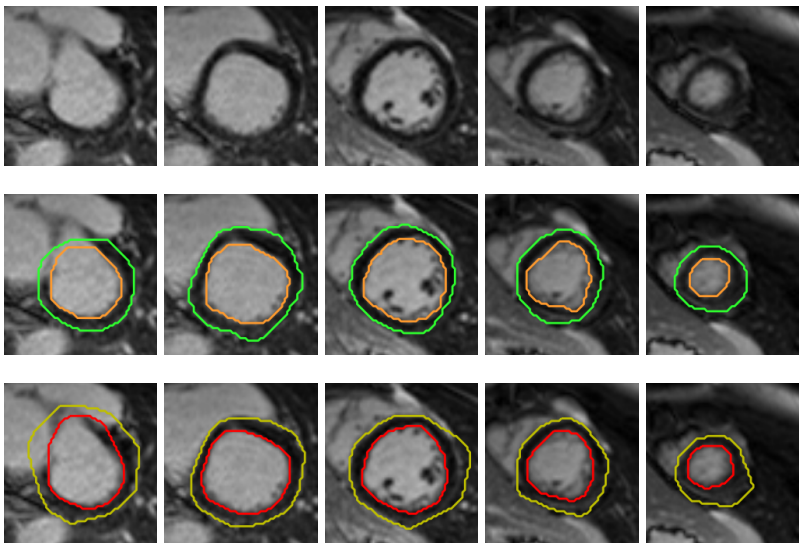

Fig. 5. Comparison of the segmentation result for one data set. From top to bottom: native slices without any contours, gold-standard annotation from clinical expert, and segmentation result of the proposed method.

The proposed method achieved a DC of 0.83 for the endocardium and epicardium. The biggest differences occur in the basal region, as the delineation of the left ventricular outflow tract is not always clear. The poor performance of the MSD is mainly due to the larger error in the apex and the left ventricular outflow tract. However, the results in the mid-cavity are convincing, which can be seen in Fig. 5. It is expected, that incorporating a model will directly improve the segmentation result.

In the course of this work, it has been shown that rather simple features can be used for the boundary detection of the endocardium and epicardium. In combination with a minimal cost path search, accurate and consistent results can be achieved. The clear benefit of the method is the independence of registration to Cine MRI and the speed.

Disclaimer: The methods and information presented in this paper are based on research and are not commercially available.

References

1. Mendis S. Global status report on noncommunicable diseases 2014. World Health Organization; 2014.
2. Petitjean C, Dacher JN. A review of segmentation methods in short axis cardiac MR images. Medical image analysis. 2011 April;15(2):169–184.

3. Suinesiaputra A, Cowan BR, Al-Agamy AO, Elattar MA, Ayache N, Fahmy AS, et al. A collaborative resource to build consensus for automated left ventricular segmentation of cardiac MR images. Medical Image Analysis. 2014 January;18(1):50–62.
4. Rashid S, Rapacchi S, Shivkumar K, Plotnik A, Finn P, Hu P. Modified wideband 3D late gadolinium enhancement (LGE) MRI for patients with implantable cardiac devices. Journal of Cardiovascular Magnetic Resonance. 2015 February;17(Suppl 1):Q26.
5. Kellman P, Arai A. Cardiac Imaging Techniques for Physicians: Late Enhancement. Journal of Magnetic Resonance Imaging. 2012 September;36(3):529–542.
6. Ciofolo C, Fradkin M, Mory B, Hautvast G, Breeuwer M. Automatic Myocardium Segmentation in Late-Enhancement MRI. In: Biomedical Imaging: From Nano to Macro, 2008. ISBI 2008. 5th IEEE International Symposium on. IEEE; 2008. p. 225–228.
7. Dikici E, ODonnell T, Setser R, White R. Quantification of Delayed Enhancement MR Images. In: Medical Image Computing and Computer-Assisted Intervention–MICCAI 2004. Springer; 2004. p. 250–257.
8. Wei D, Sun Y, Chai P, Low A, Ong SH. Myocardial Segmentation of Late Gadolinium Enhanced MR Images by Propagation of Contours from Cine MR Images. In: Medical Image Computing and Computer-Assisted Intervention–MICCAI 2011. Springer; 2011. p. 428–435.
9. Tao Q, Piers S, Lamb H, van der Geest R. Automated Left Ventricle Segmentation in Late Gadolinium-Enhanced MRI for Objective Myocardial Scar Assessment. Journal of Magnetic Resonance Imaging. 2015 August;42(2):390–399.
10. Canny J. A Computational Approach to Edge Detection. Pattern Analysis and Machine Intelligence, IEEE Transactions on. 1986 November;8(6):679–698.
11. Duda RO, Hart PE. Use of the Hough transformation to detect lines and curves in pictures. Communications of the ACM. 1972 January;15(1):11–15.
12. Lang RM, Bierig M, Devereux RB, Flachskampf FA, Foster E, Pellikka PA, et al. Recommendations for chamber quantification. European Heart Journal-Cardiovascular Imaging. 2006 February;7(2):79–108.
13. Otsu N. A Threshold Selection Method from Gray-Level Histograms. Automatica. 1979 January;11(285-296):23–27.
14. Marquez-Neila P, Baumela L, Alvarez L. A morphological approach to curvature-based evolution of curves and surfaces. Pattern Analysis and Machine Intelligence, IEEE Transactions on. 2014 January;36(1):2–17.
15. Zheng Y, Barbu A, Georgescu B, Scheuering M, Comaniciu D. Four-Chamber Heart Modeling and Automatic Segmentation for 3-D Cardiac CT Volumes Using Marginal Space Learning and Steerable Features. IEEE Transactions on Medical Imaging. 2008 November;27(11):1668–1681.
16. Qian X, Lin Y, Zhao Y, Wang J, Liu J, Zhuang X. Segmentation of myocardium from cardiac MR images using a novel dynamic programming based segmentation method. Medical Physics. 2015 March;42(3):1424–1435.
17. Dijkstra E. A Note on Two Problems in Connexion with Graphs. Numerische Mathematik. 1959;1(1):269–271.
18. Lorensen W, Cline H. Marching Cubes: A High Resolution 3D Surface Construction Algorithm. In: ACM Siggraph Computer Graphics. vol. 21. ACM; 1987. p. 163–169.
19. Wolf I, Vetter M, Wegner I, Böttger T, Nolden M, Schöbinger M, et al. The Medical Imaging Interaction Toolkit. Medical Image Analysis. 2005 December;9(6):594–604.

20. Albà X, i Ventura F, Rosa M, Lekadir K, Tobon-Gomez C, Hoogendoorn C, et al. Automatic Cardiac LV Segmentation in MRI Using Modified Graph Cuts with Smoothness and Interslice Constraints. Magnetic Resonance in Medicine. 2014 December;72(6):1775–1784.